Mapping residual strain induced by cold working and by laser shock peening using neutron transmission spectroscopy

Ramadhan, RS, Syed, AK, Tremsin, AS, Kockelmann, W, Dalgliesh, R, Chen, B, Parfitt, D & Fitzpatrick, ME

Original citation & hyperlink:
Ramadhan, RS, Syed, AK, Tremsin, AS, Kockelmann, W, Dalgliesh, R, Chen, B, Parfitt, D & Fitzpatrick, ME 2018, 'Mapping residual strain induced by cold working and by laser shock peening using neutron transmission spectroscopy' *Materials and Design*, vol 143, pp. 56-6
https://dx.doi.org/10.1016/j.matdes.2018.01.054

DOI 10.1016/j.matdes.2018.01.054
ISSN 0261-3069
ESSN 0264-1275

Publisher: Elsevier

Mapping Residual Strain Induced by Cold Working and by Laser Shock Peening using Neutron Transmission Spectroscopy

Ranggi S. Ramadhan [a,*], Abdul K. Syed [a], Anton S. Tremsin [b], Winfried Kockelmann [c], Robert Dalgliesh [c], Bo Chen [a], David Parfitt [a], Michael E. Fitzpatrick [a]

[a] *Centre for Manufacturing and Materials Engineering, Coventry University, Coventry, CV1 5FB, UK*

[b] *Space Sciences Laboratory, University of California, Berkeley, CA 94720, USA*

[c] *Rutherford Appleton Laboratory, ISIS Facility, Chilton, OX11 0QX, UK*

** Corresponding author. E-mail address: ramadhar@uni.coventry.ac.uk*

Abstract

This paper presents 2D mapping of residual strains, induced by cold expansion and laser shock peening processing of aluminium alloy samples, by using Bragg edge neutron transmission. Neutron transmission uses information contained in the neutron beam transmitted through a sample. It is shown that neutron transmission strain mapping with high spatial resolution can provide important insights into the distribution of residual strains associated with processing of materials. The residual strain field around a cold-expanded hole can be revealed in detail, as can be the residual strain profile associated with laser peening. Results are correlated with measurements obtained by conventional neutron diffraction and incremental hole drilling. The residual strain variation around the cold-expanded hole and the depth of compressive residual strain generated by the peening process were captured with high spatial resolution, showing the advantages of neutron transmission over other well-established strain measurement methods by non-destructively generating a map of residual strains over a large area.

Keywords: Neutron transmission; Residual strain; Strain mapping; Bragg edge analysis; Cold expansion; Laser shock peening

1. Introduction

Neutron transmission is a relatively new strain measurement technique, which follows similar principles to the time-of-flight neutron diffraction method, but has the potential to provide two-dimensional mapping of strains in a single measurement. It was developed in the late 1990s [1–3], but limitations in the pixel size of the detectors available at the time (typically 2 mm × 2 mm) meant that it was not pursued. Recent developments in micro-channel-plate (MCP) detector technology have allowed pixel sizes to be reduced to 50 μm × 50 μm or less.

Transmitted neutrons, having passed through a polycrystalline material, produce a spectrum that displays sharp steps in intensity as a function of neutron wavelength: these steps are the so-called Bragg edges [1]. A Bragg edge is analogous to the Bragg diffraction peak in a time-of-flight neutron diffraction measurement. As the diffracting wavelength increases for a particular set of lattice planes with spacing d, Bragg angle θ increases until it reaches 90°, where neutrons are scattered back towards the source. Above this critical wavelength, no scattering can occur from the particular lattice planes and this leads to a sharp step in transmission intensity with increasing wavelength: this is the Bragg edge. As a reminder, Bragg's law is:

$$\lambda = 2d \sin\theta \tag{1}$$

where λ is the wavelength, d is the lattice spacing, and θ is half the diffraction angle. A pixelated detector placed directly behind the sample can map the Bragg edges simultaneously for multiple positions in a sample in a single neutron beam exposure, which provides a 2D strain map [4]. Principally, a transmission detector captures the beam after passage through the sample, with some of the neutrons removed due to Bragg scattering. The Bragg edge occurs at that wavelength where the scattering condition is just fulfilled by those lattice planes perpendicular to the incident beam direction. Therefore, the strain measurement direction for Bragg edge analysis is parallel to the incoming neutron beam, and the measured strain is averaged over the path length that the neutrons have traversed in the sample. Neutron transmission offers immediate advantages over conventional

diffraction-based techniques. Spatially resolved strain data across a large area of the sample can be obtained during a single measurement using a pixelated imaging detector. Besides enabling a better illustration of the strain fields across the sample, this allows the technique to perform time-resolved observation of strain within a sample. These advantages have been highlighted by Iwase *et al.* [5] by comparing the use of Bragg edge neutron transmission and neutron diffraction to study change in lattice strain under tensile loading at different parts of the sample.

Despite its great potential, the application of neutron transmission for residual strain mapping has not been extensively explored. A small number of studies [6–8] have reported the use of this technique to measure residual strains in engineering parts. Santisteban *et al*. [6] measured residual strain in a cold-expanded hole with neutron transmission using a 10 × 10 array of 2 mm × 2 mm scintillator pixels, producing a strain map with coarse spatial resolution. Tremsin *et al.* [7] performed non-destructive examination of loads in regular and self-locking Spiralock® threads in fastened assemblies, using neutron transmission with a microchannel plate (MCP) detector. An MCP detector was also used to investigate the strain distribution across aluminium-steel and titanium-stainless steel dissimilar metal welds, where the presence of compressive residual strains at the boundary of the heat affected zone of the welds were well captured by this technique [8]. Woracek *et al*. [9] used energy-resolved neutron imaging based on a double crystal monochromator on a conventional imaging beamline to produce strains maps of steel under *in situ* loading. More recently, strain mapping extended to three dimensions has been investigated [10,11], and Lionheart and Withers [12] have highlighted the ill-posed problem for strain tomography. Whilst recent studies are taking advantage of the high spatial resolution features of neutron transmission using an MCP detector [8], there has not been thorough comparison of the measured residual strains by neutron transmission with those from other well-established measurement techniques, even for the 2D case. It is worthwhile to note that much can be learnt from the complementary uses of more than one technique for many residual stress measurement cases [13].

This paper describes the use of neutron transmission strain mapping in evaluating residual strain that is deliberately induced by different manufacturing processes. Compared to previous work, this paper also presents strain measurement results of the samples gathered by using more-established strain measurement methods. Thus, this work validates and further highlights the benefits of high-spatial-resolution strain mapping by neutron transmission.

The manufacturing processes studied are cold expansion and laser shock peening on aluminium alloys: both methods are used in the aerospace industry to enhance the fatigue performance of components. The improvements gained from the two processes highly depend on the residual strain profiles generated in the components. Here, we take full advantage of the high-spatial-resolution strain maps produced using an MCP detector to analyse the strain profiles within the components. It should be emphasised that the chosen cases and samples pose particular problems for Bragg edge analysis due to the relatively low scattering by aluminium for neutrons. Nevertheless, neutron transmission still managed to produce good strain measurement results. Neutron transmission results were compared to results from neutron diffraction and incremental hole drilling. The accuracy, advantages and limitations of the neutron transmission method are discussed.

2. Experimental details

2.1 Materials and Specimens

The first sample studied was a cold-expanded hole; a drilled hole sample was also measured as a reference. The holes were fabricated in an aluminium alloy 2624-T351 plate with 61 mm × 61 mm × 5 mm dimension. The plate width was designed to provide sufficient material to constrain deformation around the hole and to produce residual stress. The material has an elastic modulus of E = 73 GPa, and a Poisson's ratio of ν = 0.33. The cold-expanded hole was subjected to approximately 2% cold work using a split-sleeve cold expansion system, which involves pulling an

oversized mandrel, pre-fitted with a lubricated split-sleeve, through a pre-drilled fastener hole. This process started with an original hole diameter of 6.15 mm and produced a final hole diameter of 6.27 mm. The process introduces compressive residual stress adjacent to the hole in the hoop and radial directions [14,15].

The other sample type used in this study was a laser shock peened aluminium sheet, made of aluminium alloy 2024-T351 (E = 72GPa and ν = 0.3) with dimensions of 38 mm × 85 mm × 1.8 mm. In laser shock peening, short pulses of high intensity laser light are fired onto the surface of the sample, vaporizing the surface layer and producing a local plasma. Confining the plasma with a water film directs a shock wave into the material that causes plastic deformation; relaxation of the associated elastic stress field then generates compressive residual stresses at the surface [16]. An array of laser peen spots forming a line was applied along the length of the sheet, Fig. 1C, with peen spot size of 5 mm × 5 mm and power density of 1 GW/cm^2. The laser pulse duration of each spot was 18 ns, and two layers of peening were performed with 50% offset, i.e. the subsequent peen spot overlaps the previous by 50%. The elongated dimension of the laser shock peened sample was designed to provide a long transmission path for the measurement, referring to the optimum sample thickness for neutron transmission for aluminium [17], with the expectation that the residual strains are relatively constant along the length of the sample. However, the relatively low thickness of the samples, particularly the hole-containing samples, used in this study poses a challenge for neutron transmission measurement due to the low signal-to-noise obtained from aluminium with such thickness. Nonetheless these geometries are representative of those used in manufacturing service: since both cold expansion and laser shock peening are often applied to thin aluminium components such as aircraft skin.

2.2 Neutron transmission measurement setup

Neutron transmission experiments were performed at the ISIS pulsed neutron spallation source, Rutherford Appleton Laboratory, UK. The cold-expanded and drilled hole samples were measured at the ENGIN-X [18] beamline, while the laser shock peened sample was measured at the LARMOR [19] beamline. ENGIN-X uses a decoupled methane moderator and is on a 50 m flight path; a coupled hydrogen moderator is used at LARMOR which is installed on a 25 m flight path. In comparison, ENGIN-X produced sharper Bragg edges but lower neutron flux, hence needing longer time for each measurement.

The experimental setups for each of the sample types are illustrated in Fig. 1. An incident neutron beam with wavelengths ranging from 2.3-4.8 Å and 1.5-10.6 Å at ENGIN-X and LARMOR, respectively, travels through the whole thickness of the sample before arriving at the transmission detector. Each sample was placed a few millimetres in front of the detector to reduce image blurring due to beam divergence and to achieve the highest spatial resolution possible. In this study, a microchannel plate (MCP) detector [20] was used. The MCP detector uses a ^{10}B-doped plate with micro-pores as neutron-to-electron converter, followed by another micro-pored plate for electron amplification, and a 2 × 2 stack of Timepix readout chips. Each chip contains 256 × 256 pixels, with a physical pixel size of 55 μm × 55 μm. The detector provided a total field-of-view of 28 mm × 28 mm, indicated by the black, dashed line in Fig. 1.

For the cold-expanded and drilled hole samples, the samples were aligned to measure strain in both the *x*-axis direction, Fig. 1A, and *y*-axis direction, Fig. 1B, where the axes system is defined in the figure. The strain in the *x*-axis direction is the axial strain, whilst the strain in the *y*-axis direction is a mixture of hoop and radial strain depending on the position around the hole circumference, Fig. 1B. For the setup shown in Fig. 1B, the neutrons traversed quite a long path through the sample, and thus strain averaging has to be considered while analysing the result. For the laser shock peened sample, the sample was aligned to measure strain in the *x*-axis direction, Fig. 1C, parallel to the line of peen spots.

Long measurement times were required to ensure good counting statistics from the aluminium samples. Longer measurement time was especially needed in measuring the axial strain component of the cold-expanded and drilled hole samples, Fig. 1A, for which there is only a small thickness of material contributing to the scattering. The measurement time for each cold-expanded and drilled hole sample at ENGIN-X was 7.5 hours, while the measurement time of the laser shock peened sample at LARMOR was 5 hours.

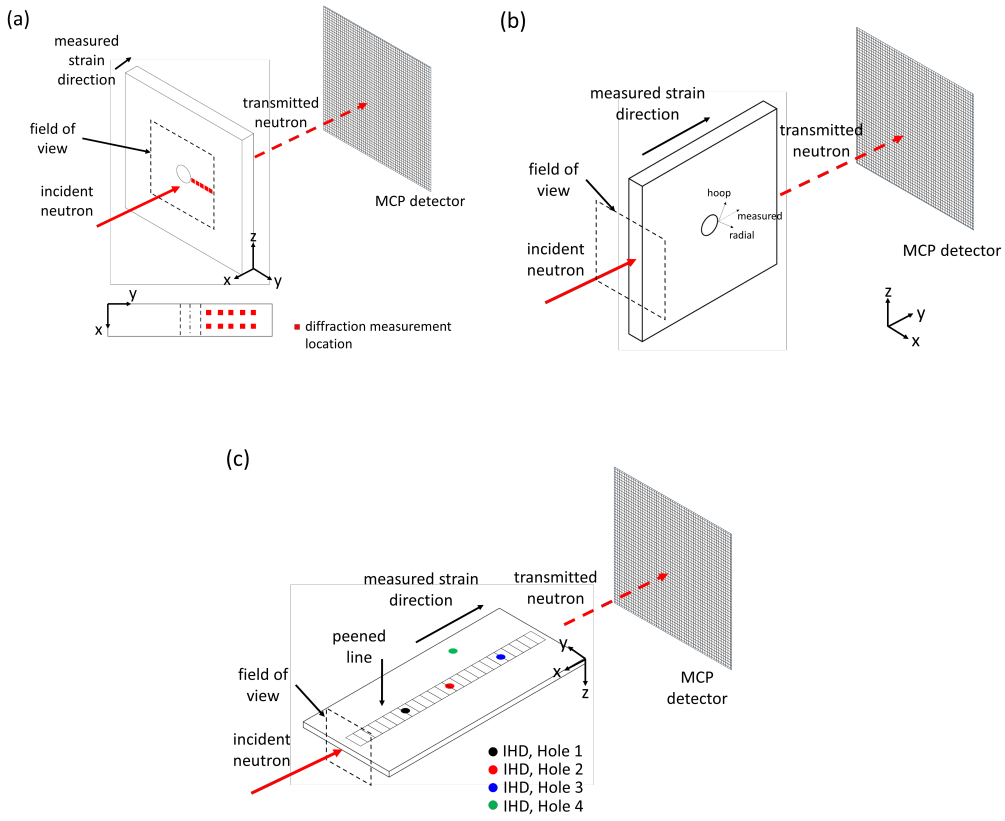

Figure 1. Experimental setup of neutron transmission for cold-expanded and drilled hole samples, with sample aligned to measure strain in: (a) *x*-axis direction, which is the axial strain direction; and (b) *y*-axis direction to provide a combination of hoop and radial strains; measurements were performed at ENGIN-X. (c) Experimental setup of neutron transmission for laser shock peened sample with sample aligned to measure strain in *x*-axis direction; measurements were performed on LARMOR. Neutron diffraction measurement points are shown in (a); IHD measurement points are shown in (b). The field-of-view for each measurement is illustrated by the black, dashed line.

2.3 Neutron transmission data analysis

To obtain a transmission spectrum for each data set, the recorded neutron spectrum was normalised by the open beam signal obtained by passing the neutron beam directly to the detector (*i.e.*, without the sample in front of the detector). This accounted for any non-uniformity in both the neutron beam intensity and the detector efficiency across the field-of-view. A typical transmission spectrum from a cold-expanded hole sample measured at ENGIN-X, and a laser shock peened sample measured at LARMOR, is shown in Fig. 2A, showing Bragg edges from the different reflection planes. At ENGIN-X, the transmission spectrum recorded only four aluminium Bragg edges, Fig. 2A, to allow finer time resolution (shorter time-of-flight/wavelength gap between signal recordings) of about 4 μs, compared to 20 μs time-bin on LARMOR. It should be noted that the total number of time-bins used with the MCP camera is 3100.

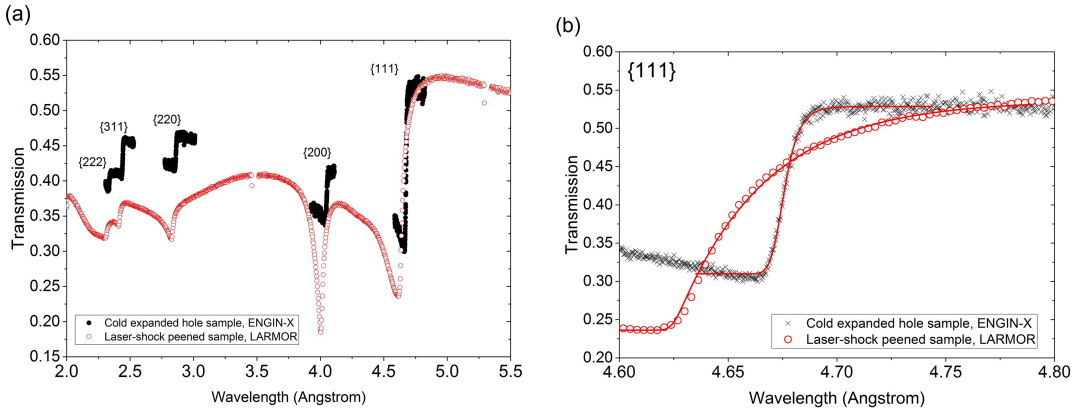

Figure 2. (a) Example of transmission spectra from the cold-expanded hole sample measured at ENGIN-X and the laser-shock peened sample measured at LARMOR. At ENGIN-X, the wavelength range settings were selected so that the detector only recorded the transmission signal from four Bragg edges, allowing finer time resolution; (b) Bragg edge from {111} plane. The points are the measured data and the solid lines are fits to the Bragg edges using Eq. 3. The ENGIN-X Bragg edge is sharper due to the characteristics of the moderator.

Single Bragg edge analysis was performed in this study by selecting the highest transmission intensity {111} Bragg edge. The elastic anisotropy of aluminium is relatively low, and consequently, there are only minor differences between strain analysis using single or multiple diffraction peaks [21]. The wavelength of the Bragg edge position, λ, was used to determine the

lattice spacing $d = \lambda/2$ of the material according to Bragg's law, Eq. 1, and then strain, ε can be calculated using Eq. 2:

$$\varepsilon = \frac{(d - d_0)}{d_0} = \frac{(\lambda - \lambda_0)}{\lambda_0} \tag{2}$$

where d_0 is the lattice spacing of a stress-free reference sample, and λ_0 is the Bragg edge position of a stress-free reference sample. Due to the availability of the beam time, a separate measurement of a stress-free reference sample was not performed. Instead, the stress-free reference Bragg edge position was taken from a region of material unaffected by cold expansion or laser peening (*i.e.*, far away from the cold-expanded or laser shock peened area).

The position of the Bragg edge was determined by fitting the neutron transmission data with an analytical function:

$$T(\lambda) = C_1 + C_2\left[efrc\left(\frac{\lambda_t - \lambda}{\sqrt{2}\sigma}\right) - \exp\left(\frac{\lambda_t - \lambda}{\tau} + \frac{\sigma^2}{2\tau^2}\right) \times efrc\left(\frac{\lambda_t - \lambda}{\sqrt{2}\sigma} + \frac{\sigma}{\sqrt{2}\tau}\right)\right] \tag{3}$$

where $T(\lambda)$ is transmission intensity at neutron wavelength λ, λ_t is the edge position, σ and τ define the broadening components of the edge. C_1 and C_2 are constants which are, however, fitted in the process. The solid lines in Fig. 2B show the fitting results on {111} aluminium Bragg edges, with a derived fitting error of 1.85×10^{-3} Å and 7.04×10^{-3} Å for the Bragg edge position of the cold-expanded hole and laser shock peened sample, respectively. These two fitting error values are equivalent to 39 and 151 με, respectively.

Strain mapping was performed by fitting the Bragg edges for all pixels on the data set using Eq. 3. Before fitting, neutron counts from several neighbouring pixels were combined into one

spectrum to achieve improved counting statistics. The size of this combined area, called the 'box' or 'macropixel', was between 1.10 mm × 1.10 mm to 2.75 mm × 2.75 mm, and the fitted λ value was assigned to the centroid of the box. The maps were then produced with a step size of 55 μm using the 'running average' of this box. This combined pixel imaging analysis approach for producing strain maps is described in [8]. It involves a running average that has a similar effect like smoothing the ideal strain map with a Gaussian filter, and yields an effective spatial resolution within a range of few hundred microns. In addition, the geometric blurring owing to the divergence of the beam has to be considered which for our sample size, for an estimated *L/D* of 150 and a sample size of 85 mm, is about 0.5 mm. In this report, the strain maps shown in Fig. 3 should have more significant blurring compared to the strain maps in Fig. 5 and Fig. 6 due to a larger macropixel box size being applied.

2.4 Neutron diffraction measurement

Neutron diffraction was performed on the cold-expanded hole sample at ENGIN-X. Point-to-point neutron diffraction spectra were obtained using a gauge volume of 2 mm × 2 mm × 2 mm. Measurements were performed at two different thickness locations: x = 1.5 mm and x = 3.5 mm from the sample surface, Fig. 1A. At each thickness, five measurements were performed along the y-axis at 1.5 mm, 3 mm, 4.5 mm, 6 mm, and 7.5 mm away from the edge of the cold-expanded hole. Multiple diffraction peaks were recorded and Pawley-type full pattern refinements for determining the lattice parameters were performed to determine the lattice parameters. A stress-free reference sample was prepared by extracting a 3 mm × 3 mm × 3 mm cube from the edge of the measured aluminium plate (*i.e.*, away from the hole). Lattice parameters from the measurement points on the sample and the stress-free reference sample were then used to calculate the residual strain, producing strain values with uncertainties within 50 με. The derived residual strains from the two measurement lines from different thickness locations, Fig. 1A, were then averaged. Neutron

diffraction measurements were performed prior to the neutron transmission measurements. A comparison between the axial strains measured by neutron diffraction and by neutron transmission is reported in the following sections.

2.5 Incremental hole drilling measurement

Incremental hole drilling (IHD) measurements were performed on the laser shock peened sample. Before the measurements, the laser shock peened sample was adhesively bonded to a resin backing to prevent distortion during drilling. Three holes were drilled at different positions along the peened line, and one hole was drilled on the unpeened part of the sample, approximately 5 mm away from the middle of the peened line, as shown in Fig. 1C. The final drilled hole diameter was measured to be between 1.85-1.95 mm. Strain relaxation was measured using a standard three-gauge rosette: two gauges separated by 90˚ to measure strain in the *x* and *y*-axis directions, and one at 45°. All measurements were performed using an IHD measurement system developed by Stresscraft, UK, and according to the UK National Physical Laboratory Good Practice Guide [22]. To interpret the data and convert the relaxed strains at various depths within the sample to the corresponding stresses, the integral method was applied [22] using Stresscraft RS INT 5.1.2 software.

The in-plane stresses in the *x*- and *y*-axis directions from IHD measurements were used to back-calculate the *x*-axis direction strain using Hooke's law, assuming stress in the *z*-axis direction is zero (plane stress). Then, the calculated *x*-axis direction strain was compared with the strain measured by neutron transmission. The IHD measurement was performed after the non-destructive neutron transmission measurement on the laser shock peened sample.

3. Results

3.1 Cold-expanded and drilled hole samples

The strain maps presented in Fig. 3 show the comparison between residual strain fields for cold-expanded and drilled holes in the axial strain direction, measured with neutron transmission. A significant difference is seen between the residual strain distribution around the cold-expanded hole, Fig. 3A and the drilled hole, Fig. 3B. Pronounced tensile residual strain, with magnitude of up to around 3000 με was observed around the circumference of the cold-expanded hole, Fig. 3A. Such high tensile residual strain was not found for the drilled holes, Fig. 3B, where the residual strains around the circumference of the drilled hole were similar to those over the rest of the area of the sample. The tensile residual strain in the axial direction for the cold-expanded hole can be explained by the Poisson effect. As the mandrel used in the cold expansion process is removed, the elastic bulk of material surrounding the hole springs back and generates compressive strain in the vicinity of the hole in the hoop and radial directions. In the axial direction, which is perpendicular to the hoop and radial directions, tensile strain is generated owing to the Poisson effect. This finding is consistent with neutron diffraction measurement results by Edwards and Ozdemir [15], and neutron transmission results by Santisteban [6].

Strain asymmetry around the cold-expanded hole sample can also be observed in Fig. 3A, where there are regions of high and low tensile residual strain around the circumference of the hole. A line profile of axial residual strain was extracted from the map shown in Fig. 3A, to provide more detailed information about the strain asymmetry. Four lines, A, B, C and D, each 90° apart, indicate the location from where the strain profiles were extracted: see the inset in Fig. 4. It can be observed from Fig. 4 that the strain profile taken from line B has significantly lower tensile strain compared to those taken from lines A, C and D, especially close to the hole edge. At a distance of 500 μm from the hole edge, the magnitude of residual strain at line B is around 500 με, whilst at the same distance the magnitudes are around 2300, 2800, and 1700 με for lines A, C and D, respectively. This residual strain asymmetry phenomenon is consistent with findings from finite-element simulation [23]. The asymmetry of the strains around the cold-expanded hole is a result of the gap

in the split-sleeve used to facilitate the passage of the mandrel through the hole during the expansion process. During the expansion process, radial pressure is introduced by the oversized mandrel to the plate via the sleeve. On the opening of the sleeve, however, there is a lack of pressure on the plate. This leads to a low residual stress region in the sleeve opening area. Although the details of sleeve opening position was not available for the particular sample, the hypothesis is that B was the sleeve opening position and therefore exhibits lower strain values.

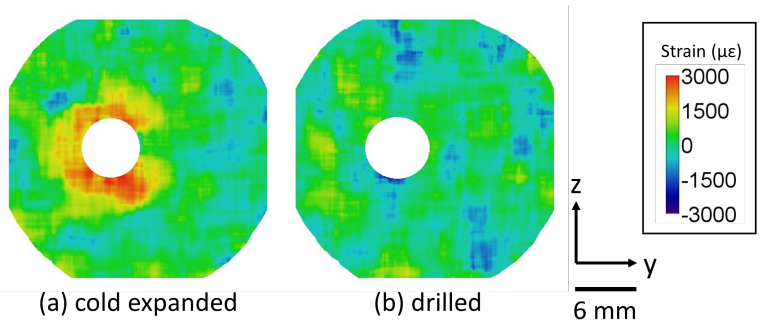

Figure 3. Residual strain map of (a) cold-expanded sample and (b) drilled hole sample. The strain measured is the axial (*z*) strain. Tensile residual strain is detected around the cold-expanded hole, but not around the drilled hole. Strain asymmetry can be observed around the circumference of the cold-expanded hole.

Neutron diffraction measurements were performed on the cold-expanded hole sample. The axial strains measured using neutron diffraction were then compared with those measured using neutron transmission and are plotted in Fig. 4. The locations of the neutron diffraction measurement points relative to the strain map are shown in the inset of Fig. 4. Also in Fig. 4 are residual strains from a cold-expanded hole measured using the Sachs boring method by Edwards and Ozdemir [24]. Their study reports hoop, radial, and axial residual stresses on a 4% cold-expanded hole in 7000-series aluminium alloy [24], and here axial strain was back-calculated using Hooke's Law. From Fig. 4, it can be seen that the neutron diffraction results are consistent with neutron transmission results taken from the same position, shown by line B. Both results show low tensile residual strain below 1000 με close to the hole edge, and gradually approach zero strain as a function of distance away from the hole. Meanwhile, axial residual strains measured using the

Sachs boring method show high tensile strain close to the hole edge, and more closely resemble the neutron transmission results measured at lines A, C, and D, Fig. 4.

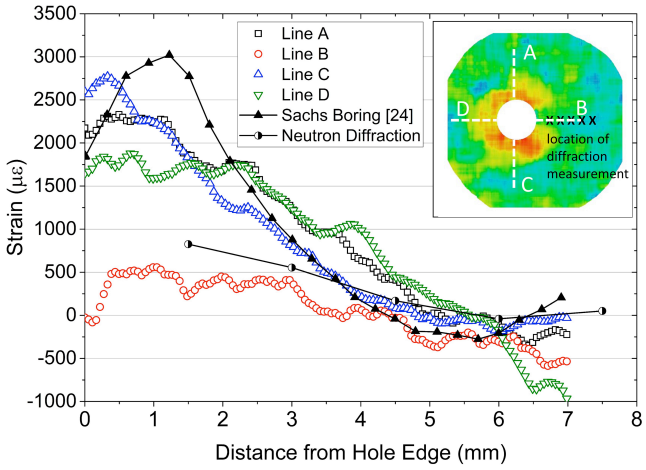

Figure 4. Residual axial strain profile of a cold-expanded hole, extracted from the strain map shown in figure 3A, and comparison between the neutron transmission and neutron diffraction results. The location from where the strain profiles were extracted is shown in the inset. Strain asymmetry around the circumference of the hole can be observed, where measurement on line B shows significantly lower residual strain compared to lines A, C and D. Previous literature values measured using the Sachs boring method [24] on a similar sample are also shown for comparison. Good agreement is observed between the neutron diffraction and transmission results measured on line B. The Sachs boring method has similar magnitude and trend with neutron transmission result on lines A, C and D.

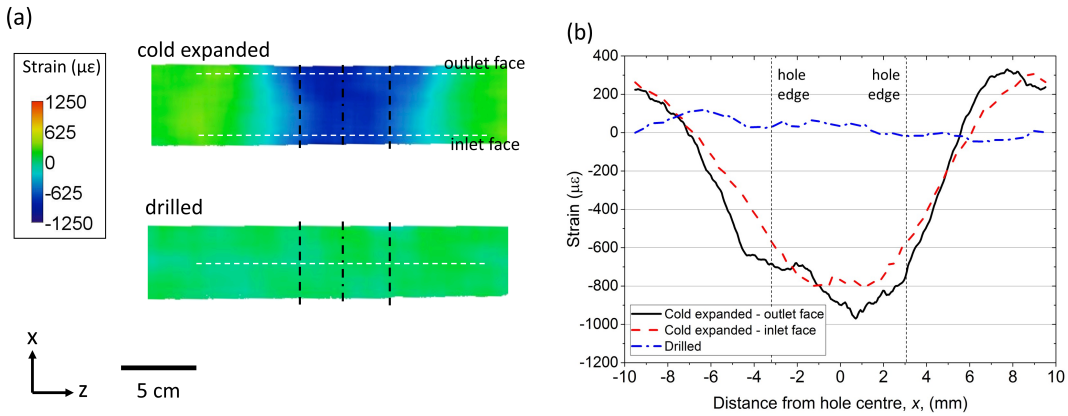

Figure 5. (a) Residual strain of the cold-expanded hole and the drilled hole sample, with measured strain in the *y*-axis direction. The black dashed line shows the approximate hole edge position. Compressive residual strain was measured around the cold-expanded hole, while near-zero strain is observed around the drilled hole; (b) Strain profiles taken from the positions shown by the dashed lines in (a). Strain values on the outlet face are slightly more compressive compared to the inlet face.

Fig. 5A shows the 2D residual strain map around cold-expanded and drilled holes in the *y*-axis direction, using the experimental setup and coordinate system shown in Fig. 1B. This *y*-axis direction strain is a combination of hoop and radial strain depending on the location of the measurement relative to the hole edge. The approximate location of the cold-expanded and drilled holes is shown by the black, dashed line in Fig. 5A. It can be clearly seen that there is significant difference between the residual strain around the cold-expanded hole and drilled holes, Fig. 5A. Compressive residual strains are present in the vicinity of the cold-expanded hole, while almost zero strain is observed around the drilled hole. Line profiles of residual strain were extracted from the 2D map: at the mandrel inlet face and outlet face of the cold-expanded hole, and also from the middle of the plate of the drilled hole sample, as shown by the white, dashed lines in Fig. 5A. The line profiles are plotted in Fig. 5B. The outlet face of the cold-expanded hole has slightly higher compressive residual strain compared to the inlet face with average difference around 100 με, Fig. 5B, while the strains become tensile at distance of 1.5-2 mm away from the hole edge. The residual strain around the drilled hole fluctuates around zero strain, Fig. 5B.

3.2 Laser shock peened sample

The 2D map of *x*-axis direction residual strain in the laser shock peened sample is shown in Fig. 6A. The 2D map was obtained from the experimental setup shown in Fig. 1C. The map clearly shows the compressive residual strain below the peened surface. To obtain more detailed information, line profiles of strains were extracted from the 2D map. Three horizontal lines A, B, and C show the locations from where the strain profiles were extracted, at different depths from the peened surface, z = 0.11 mm, 0.44 mm and 1.25 mm, respectively. The corresponding residual strain profiles are shown in Fig. 6B. The highest compressive residual strain of around –1400 με is observed at z = 0.44 mm, while compressive strains at z = 0.11 and 1.25 mm have maximum values of –1250 με and –900 με respectively, Fig. 6B. Another observation from Fig. 6B is the shape of

the maximum compressive strain area generated by the laser shock peening process. At both z = 0.11 mm and 0.44 mm, there is an area at the centre of the peen spot where the compressive strain is a maximum and does not vary with position. At the edges of this area, the compressive strain sharply decreases and moves towards tensile strain. In this study, this area is specified as the effective peened area. It can also be observed that at z = 0.11 mm, tensile residual strain is observed on the outer edge of the peened area, Fig. 6B. This corresponds to the balancing strain accommodating the compressive strain in the peened region.

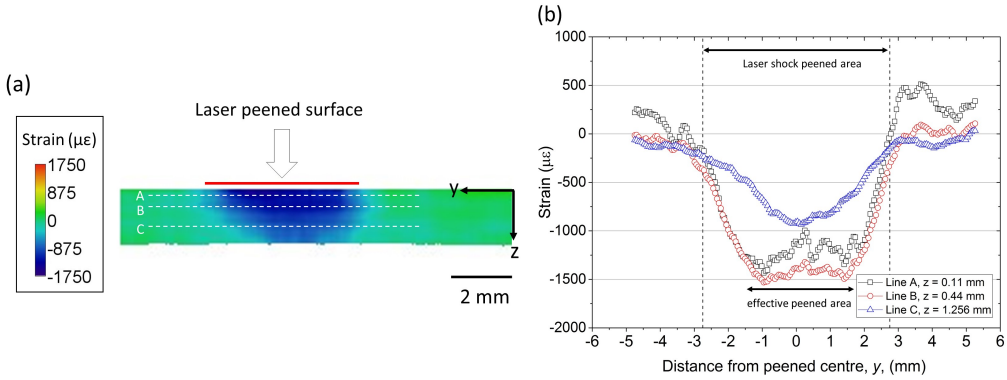

Figure 6. (a) In-plane strain map from the laser-shock peened sample, showing compressive residual strain directly below the peened surface. The white dashed lines, labelled A, B, and C, show the positions of line profiles of strain; (b) line profiles from lines A, B and C, showing the strain profile at various depths. The effective width of the peened area can be observed.

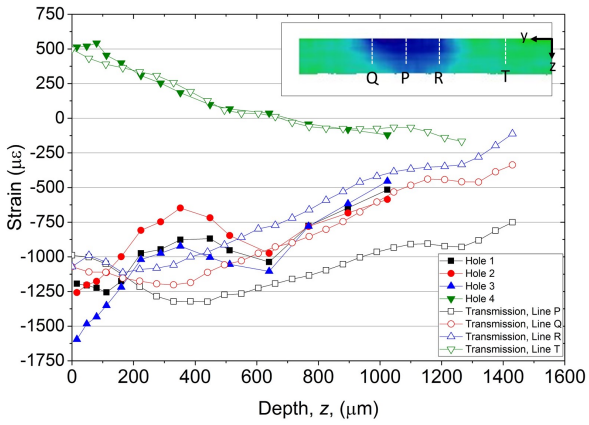

Figure 7. Comparison between IHD results and neutron transmission results. Strain profiles from neutron transmission are taken from the 2D strain map at the locations shown by the white dashed lines in the inset, labelled P, Q, R and T. Strain profiles from IHD and neutron transmission show good agreement, both on the peened and unpeened areas.

Fig. 7 shows a comparison between neutron transmission and IHD results for the laser shock peened sample. Four IHD measurements with locations shown in Fig. 1C are plotted against line profiles extracted from the 2D residual strain map which was shown previously in Fig. 6A. The locations from where the line profiles were extracted are shown in the inset of Fig. 7, labelled lines P, Q, R and T. Line P was drawn at the centre of the peen spot, lines Q and R were drawn 2 mm to the left and right of line P, respectively, and line T was drawn in the unpeened part of the sample. IHD measurements at Hole 1 and Hole 2 show a maximum compressive residual strain of around –1250 με in the first 100 μm below the peened surface, Fig. 7. Further away from the peened surface, the strain fluctuates but overall moves towards tensile strain. Higher compressive residual strain is observed from IHD measurement at Hole 3, with compressive residual strain of around –1600 με close to the peened surface. The strain then gradually moves towards tensile strain with increasing distance from the peened surface, Fig. 7. The variation of peak compressive strain along the peen line can be attributed to the strain variation which occurs between the centre and the edge of the peen spot [16]. Nevertheless, the magnitude and trends of the IHD results are within the range of the neutron transmission residual strain results. At the centre of the peen spot, line P, neutron transmission measures a maximum compressive residual strain of –1250 με at a depth of z = 400 μm below the peened surface, Fig. 7. The strain moves towards tensile strain with increasing distance from the peened surface. Similar trends are observed on the strain profiles taken from line Q and R, but with lower compressive strain magnitude. Interestingly, the IHD results measured on Hole 4 have almost perfect agreement with the neutron transmission results from line T, where the two measurements were taken from the unpeened part of the sample. Both results show tensile strain at the surface with magnitude of around 500 με, and gradually move towards zero strain with increasing distance from the sample surface, Fig. 7. As mentioned before, the tensile strain on the unpeened part of the sample is most likely the balancing strain to the compressive residual strain from the peening.

4. Discussion

The high spatial resolution and relatively large area of the strain map obtained in this work, made possible by the MCP detector, allow us to capture strain features previously not accessible using a neutron technique. For example, a full map of residual strain generated by the laser shock peening process on a 1.8-mm-thick plate can be reconstructed, Fig. 6, and the strain profile can be plotted as a function of position through the sample thickness, Fig. 7. The strain gradient in such a thin plate cannot be obtained using a detector with a pixel size of 2 mm × 2 mm [6], that was the best available technology when the technique was first explored in the 1990s. Synchrotron X-ray diffraction can offer the required spatial resolution, but can face challenges in aluminium alloys because of texture effects, and the synchrotron X-ray diffraction method also has challenges associated with strain averaging because of the elongated gauge volume that is a consequence of the high photon energy. Sub-mm spatial resolution also provides more detail on residual strain generated around cold-expanded holes, considering most of the residual strain magnitude has diminished within a distance of 1-2 mm away from the hole edge, Fig. 4.

High-spatial-resolution 2D strain mapping provides more information on residual strain fields compared to 1D strain results obtained by other measurement techniques. This becomes the key advantage of neutron transmission strain mapping over, in this case, neutron diffraction and incremental hole drilling. In this study, neutron transmission revealed the strain asymmetry around the circumference of cold-expanded holes as shown by the strain maps in Fig. 3A and 3B and the strain plot in Fig. 4. Strain asymmetry around cold-expanded holes, specifically using the split-sleeve cold expansion system, has been reported in previous studies. Some authors attribute this phenomenon to the lack of pressure at the opening of the split-sleeve, which results in a low

residual stress at that position [23,25]; however, results from other studies contradict this assumption [14,26]. This disagreement in results underlines the challenge of measuring residual strain around cold-expanded holes using conventional techniques that have relatively low spatial resolution. Using X-ray or neutron diffraction, where strain information needs to be harvested point-by-point across the sample, evaluating strain asymmetry around a cold-expanded hole is very time consuming. Moreover, a comparison of only a subset of data can lead to significant discrepancies between calculated values. For example, without any prior knowledge of the strain profile around a cold-expanded hole, a series of neutron diffraction measurements with line-shaped array of measurement points, or the Sachs boring method with a strain gauge attached at only one angular position around the cold-expanded hole, may only pick up strain from the low-strain region, Fig. 4. In this case, neutron transmission provides a complementary technique with the ability to produce a representative strain distribution around the cold-expanded hole with a single measurement. The information can then be used to determine the location of multi-direction strain scanning, for example using X-ray or neutron diffraction, to obtain a full residual stress profile.

Another example of the advantage presented by neutron transmission strain mapping is the ability to investigate the effective peened area generated by laser shock peening, Fig. 6. This information is important since the result from this study indicates that the effective peened area can be smaller than the size of the peen spots. Therefore, significant overlap between peen spots is needed to achieve a homogeneous compressive stress across the area covered by an array of peen spots. Such information cannot be obtained by IHD measurement across the peen line, since there is a minimum distance required between adjacent holes owing to local strain relaxation. Neutron diffraction would also be limited by the size of the gauge volume in obtaining such information, which is typically of linear dimension of at least 1 mm. Synchrotron X-ray diffraction has been used to study the strain across peen spots [16], but many measurement points are needed.

Alongside the benefits of 2D strain mapping, however, the through-thickness averaging nature of neutron transmission strain measurement must be considered when interpreting the results. The values in the strain maps are through-thickness averages, i.e. neutron transmission is insensitive to the spatial variation of strain along the averaging direction (i.e. the incoming beam direction). This can be observed while analysing the laser shock peened sample. The sample has significant strain oscillation along the peen line, where higher compressive strains are measured at the edges in-between peen spots compared to those at the centre of the spots [16]. This phenomenon was captured by IHD measurements, as different measurement points along the peen line showed different compressive strain magnitudes, particularly near the surface, Fig. 7. In the neutron transmission strain map, this variation is averaged. Therefore, on the peened part of the laser shock peened sample, the differences between IHD and neutron transmission measurements are more pronounced, Fig. 7. However, the agreement between neutron transmission and IHD results are generally good. Another example is the measurement of residual strains on the mandrel inlet and outlet faces of a cold-expanded hole, Fig. 5. There is consensus that the magnitude of compressive residual stress is higher at the outlet face compared to the inlet face, owing to the constraint at the outlet surface causing more deformation as the mandrel is pulled through the hole [27,28]. This phenomenon was captured by neutron transmission, Fig. 5B, where the outlet face of the cold-expanded hole showed slightly higher compressive residual strain compared to the inlet face. However, the difference is only about 100 με, which is within the uncertainty of the measurement. Also, this in-plane compressive residual strain is generally lower in magnitude compared to the out-of-plane tensile residual strain. This can be attributed to the fact that the strains are averaged through the thickness of the sample, including regions that are far away from the cold-expanded hole. Averaging decreases the sensitivity to measure strain accurately in this particular orientation.

The comparison between neutron transmission, neutron diffraction and IHD performed in this study provides an estimate of the accuracy of neutron transmission strain measurement. Good

agreement is found between neutron diffraction and neutron transmission measurements on measuring the strain around a cold-expanded hole. The average difference between neutron transmission and neutron diffraction results in this case was less than 250 με, Fig. 4; and this difference can be attributed to several factors. The first one is the difference in the size and shape of the gauge volume over which the measurements were taken The strains measured by neutron diffraction were averaged over a 2 mm × 2 mm × 2 mm gauge volume, whilst those measured by neutron transmission were averaged over the area made by the combined pixels, and through the thickness of the sample. The other explanation for this difference is the different method of obtaining the stress-free reference value. A small cube of the sample was taken as reference sample in neutron diffraction measurement, whilst an arbitrary region far away from the hole was selected as the reference in neutron transmission measurement. As a result of the different approaches to determine the stress-free reference, there could be an offset between the results from the two measurements. However, relative strain variation across the sample presented by the two measurements should be consistent. This is shown to be the case in Fig. 4, between line B of neutron transmission and neutron diffraction result.

Good agreement was also observed between the neutron transmission and IHD on the unpeened area of the laser shock peened sample where tensile strain around 500 με on the surface was observed, with an average difference less than 100 με, Fig. 7. This agreement is a valuable result considering IHD and neutron transmission use completely different principles in measuring residual strain. The agreement of the neutron transmission results with other, more established strain measurement methods demonstrates the efficacy of neutron transmission as a strain measurement tool. The agreement also shows that selecting part of the sample approximately 15 mm away from the peened area as a reference value in calculating strain is a good approximation.

It is also worth noting that aluminium has a low coherent scattering cross section for neutrons, and this presents difficulties in terms of getting good statistics for the Bragg edge signal for samples

that are relatively thin. Results from this study show that 5-7.5 hours of measurement time is sufficient to obtain a good Bragg edge signal from aluminium alloy with minimum thickness of 5 mm along the transmission direction, and allows the subsequent characterisation of strain, Fig. 2B. Having sharper Bragg edges due to the characteristics of the moderator, ENGIN-X was able to produce better strain resolution with fitting uncertainties of around 40 με, but at the expense of lower neutron flux and thus longer measurement time to achieve good counting statistics. The LARMOR instrument, in comparison, can perform measurements faster with higher flux, but has broader Bragg edges and produced results with higher uncertainty of around 150 με. There is scope to substantially reduce measurement time, both with development in detector technology and the operation of the new, dedicated imaging beamline IMAT at ISIS [29]. Several options in characterising and fitting the Bragg edge and improving the accuracy of measuring the edge shifts are also promising areas for further investigation to improve both the accuracy of the strain measurements and maximise the additional data that may be obtained from the Bragg edges. Since the current strain maps were reconstructed from single Bragg edges, the inclusion of higher index planes by concurrent fitting of multiple Bragg edges may also improve the sensitivity of the technique with regards to small variations of the residual stresses.

Conclusions

1. Using micro-channel-plate detector technology, 2D residual strain mapping has been performed using the neutron transmission technique, generating strain maps with practical spatial resolution of a few hundred microns. The value of this high spatial resolution has been demonstrated through mapping of strain gradients through the thickness of a 1.8-mm-thick laser shock peened plate; and measurement of the strain field around a cold-worked hole; both in aluminium alloys. Such measurements are of particular value in aerospace applications where detailed knowledge of the residual stress field is important.

2. Results from the neutron transmission method were compared to measurements from conventional neutron diffraction. The discrepancy between the neutron transmission technique and the other well-established technique is within 100-250 με, which is more than acceptable given the different volume averaging of the two techniques. Therefore, neutron transmission strain mapping can complement conventional strain measurement techniques.
3. The variation of tensile axial residual strain around a cold-expanded hole, which is a Poisson strain from the cold expanding process, was observed using neutron transmission with highest peak strain value of around 2800 με and lowest peak strain value of around 500 με.
4. Using neutron transmission, compressive residual strain of around –1400 με was observed at a depth of around 400 μm from the surface of a laser shock peened sample.
5. Although there is a limitation in detecting spatial variation of strain in the measurement direction as a consequence of the averaging of strain along the beam path, neutron transmission strain mapping has been proven to provide valuable additional data of residual strains in engineering samples. Better result can be achieved in future by improvements in neutron transmission instrumentation, transmission detector technology, and Bragg edge data analysis.

Acknowledgements

RSR is supported by an ISIS Facility Development Studentship, and we are grateful for funding to the UK Science and Technology Facilities Council (STFC). MEF is grateful for funding from the Lloyd's Register Foundation, a charitable foundation helping to protect life and property by supporting engineering-related education, public engagement and the application of research.

Reference

[1] A. Steuwer, P.J. Withers, J.R. Santisteban, L. Edwards, G. Bruno, M.E. Fitzpatrick, M.R. Daymond, M.W. Johnson, D. Wang, Bragg Edge Determination for Accurate Lattice Parameter and Elastic Strain Measurement, Phys. Status Solidi Appl. Res. 185 (2001) 221–230. doi:10.1002/1521-396X(200106)185:2<221::AID-

PSSA221>3.0.CO;2-C.
[2] J.R. Santisteban, L. Edwards, M.E. Fitzpatrick, A. Steuwer, P.J. Withers, M.R. Daymond, M.W. Johnson, N. Rhodes, E.M. Schooneveld, Strain imaging by Bragg edge neutron transmission, Nucl. Instruments Methods Phys. Res. Sect. A Accel. Spectrometers, Detect. Assoc. Equip. 481 (2002) 765–768. doi:10.1016/S0168-9002(01)01256-6.
[3] S. Vogel, A Rietveld-Approach for the Analysis of Neutron Time-of-Flight Transmission Data, Christian-Albrechts-Universität zu Kiel, 2000.
[4] A.S. Tremsin, J.B. McPhate, J. V. Vallerga, O.H.W. Siegmund, W. Kockelmann, A. Steuwer, W.B. Feller, High-resolution neutron counting sensor in strain mapping through transmission Bragg edge diffraction, IEEE Sens. J. 11 (2011) 3433–3436. doi:10.1109/JSEN.2011.2160339.
[5] K. Iwase, H. Sato, S. Harjo, T. Kamiyama, T. Ito, S. Takata, K. Aizawa, Y. Kiyanagi, In situ lattice strain mapping during tensile loading using the neutron transmission and diffraction methods, J. Appl. Crystallogr. 45 (2012) 113–118. doi:10.1107/S0021889812000076.
[6] J.R. Santisteban, L. Edwards, M.E. Fizpatrick, A. Steuwer, P.J. Withers, Engineering applications of Bragg-edge neutron transmission, Appl. Phys. A Mater. Sci. Process. 74 (2002) 1433–1437. doi:10.1007/s003390101241.
[7] A.S. Tremsin, T.Y. Yau, W. Kockelmann, Non-destructive Examination of Loads in Regular and Self-locking Spiralock ® Threads through Energy- resolved Neutron Imaging, Strain. 52 (2016) 548–558. doi:10.1111/str.12201.
[8] A.S. Tremsin, S. Ganguly, S.M. Meco, G.R. Pardal, T. Shinohara, W.B. Feller, Investigation of dissimilar metal welds by energy-resolved neutron imaging, J. Appl. Crystallogr. 49 (2016) 1130–1140. doi:10.1107/S1600576716006725.
[9] R. Woracek, D. Penumadu, N. Kardjilov, A. Hilger, M. Strobl, R.C. Wimpory, I. Manke, J. Banhart, Neutron Bragg-edge-imaging for strain mapping under in situ tensile loading, J. Appl. Phys. 109 (2011) 2–6. doi:10.1063/1.3582138.
[10] J.N. Hendriks, A.W.T. Gregg, C.M. Wensrich, A.S. Tremsin, T. Shinohara, M. Meylan, E.H. Kisi, V. Luzin, O. Kirsten, Bragg-edge elastic strain tomography for *in situ* systems from energy-resolved neutron transmission imaging, Phys. Rev. Mater. 1 (2017) 53802. doi:10.1103/PhysRevMaterials.1.053802.
[11] B. Abbey, S.Y. Zhang, W. Vorster, A.M. Korsunsky, Reconstruction of axisymmetric strain distributions via neutron strain tomography, Nucl. Instruments Methods Phys. Res. Sect. B Beam Interact. with Mater. Atoms. 270 (2012) 28–35. doi:10.1016/j.nimb.2011.09.012.
[12] W.R.B. Lionheart, P.J. Withers, Diffraction tomography of strain, Inverse Probl. 31 (2015) 45005. doi:10.1088/0266-5611/31/4/045005.
[13] P.J. Withers, H.K.D.H. Bhadeshia, Residual stress. Part 1–measurement techniques, Mater. Sci. Technol. 17 (2001) 355–365. doi:10.1179/026708301101509980.
[14] R. Cook, P. Holdway, Residual stresses induced by hole cold expansion, Trans. Eng. Sci. 2 (1993) 91–100.
[15] L. Edwards, A.T. Ozdemir, Residual Stresses at Cold Expanded Fastener Holes, in: M.T. Hutchings, A.D. Krawitz (Eds.), Meas. Residual Appl. Stress Using Neutron Diffr., Springer Science+Business Media, B.V., 1992: pp. 545–554.
[16] M. Dorman, M.B. Toparli, N. Smyth, A. Cini, M.E. Fitzpatrick, P.E. Irving, Effect of laser shock peening on residual stress and fatigue life of clad 2024 aluminium sheet containing scribe defects, Mater. Sci. Eng. A. 548 (2012) 142–151. doi:10.1016/j.msea.2012.04.002.
[17] J.R. Santisteban, L. Edwards, A. Steuwer, P.J. Withers, Time-of-flight neutron

transmission diffraction, J. Appl. Crystallogr. 34 (2001) 289–297. doi:10.1107/S0021889801003260.
[18] J.R. Santisteban, M.R. Daymond, J.A. James, L. Edwards, ENGIN-X: A third-generation neutron strain scanner, J. Appl. Crystallogr. 39 (2006) 812–825. doi:10.1107/S0021889806042245.
[19] ISIS Larmor, (n.d.). https://www.isis.stfc.ac.uk/Pages/Larmor.aspx (accessed October 1, 2017).
[20] A.S. Tremsin, J. V. Vallerga, J.B. McPhate, O.H.W. Siegmund, Optimization of high count rate event counting detector with Microchannel Plates and quad Timepix readout, Nucl. Instruments Methods Phys. Res. Sect. A Accel. Spectrometers, Detect. Assoc. Equip. 787 (2015) 20–25. doi:10.1016/j.nima.2014.10.047.
[21] M.R. Daymond, M.W. Johnson, D.S. Sivia, Analysis of neutron diffraction strain measurement data from a round robin sample, J. Strain Anal. 37 (2002) 73–85.
[22] P. V Grant, J.D. Lord, P. Whitehead, The Measurement of Residual Stresses by the Incremental Hole Drilling Technique, 2006.
[23] V. Nigrelli, S. Pasta, Finite-element simulation of residual stress induced by split-sleeve cold-expansion process of holes, J. Mater. Process. Technol. 205 (2008) 290–296. doi:10.1016/j.jmatprotec.2007.11.207.
[24] L. Edwards, A.T. Ozdemir, Effect of residual stress on fatigue life of cold expanded fastener holes, Trans. Eng. Sci. 2 (1993) 101–109.
[25] A. Cirello, S. Pasta, Displacement measurement through digital image correlation and digital speckle pattern interferometry techniques in cold-expanded holes, Strain. 46 (2010) 581–588. doi:10.1111/j.1475-1305.2008.00469.x.
[26] A.A. Garcia-Granada, V. Lacarac, D.J. Smith, M.J. Pavier, R. Cook, P. Holdway, 3D residual stress around cold expanded holes in a new creep resistant aluminium alloy, Trans. Eng. Sci. 25 (1999) 103–116.
[27] Y. Zhang, M.E. Fitzpatrick, L. Edwards, Analysis of the residual stress around a cold-expanded fastener hole in a finite plate, Strain. 41 (2005) 59–70. doi:10.1111/j.1475-1305.2005.00181.x.
[28] T.N. Chakherlou, M. Shakouri, A.B. Aghdam, A. Akbari, Effect of cold expansion on the fatigue life of Al 2024-T3 in double shear lap joints: Experimental and numerical investigations, Mater. Des. 33 (2012) 185–196. doi:10.1016/j.matdes.2011.07.024.
[29] T. Minniti, K. Watanabe, G. Burca, D.E. Pooley, W. Kockelmann, Characterization of the new neutron imaging and materials science facility IMAT, Nucl. Instruments Methods Phys. Res. (2017).